

Investigating the Relationship between the Evaporative Stress Index and Land Surface Conditions in the Contiguous United States

YAFANG ZHONG AND JASON A. OTKIN

*Space Science and Engineering Center, Cooperative Institute for Meteorological Satellite Studies,
University of Wisconsin–Madison, Madison, Wisconsin*

MARTHA C. ANDERSON

Hydrology and Remote Sensing Laboratory, Agricultural Research Service, USDA, Beltsville, Maryland

CHRISTOPHER HAIN

Earth Science Branch, NASA Marshall Space Flight Center, Huntsville, Alabama

(Manuscript received 6 September 2019, in final form 7 May 2020)

ABSTRACT

Despite the key importance of soil moisture–evapotranspiration (ET) coupling in the climate system, limited availability of soil moisture and ET observations poses a major impediment for investigation of this coupling regarding spatiotemporal characteristics and potential modifications under climate change. To better understand and quantify soil moisture–ET coupling and relevant processes, this study takes advantage of in situ soil moisture observations from the U.S. Climate Reference Network (USCRN) for the time period of 2010–17 and a satellite-derived version of the evapotranspiration stress index (ESI), which represents anomalies in a normalized ratio of actual to reference ET. The analyses reveal strong seasonality and regional characteristics of the ESI–land surface interactions across the United States, with the strongest control of soil moisture on the ESI found in the southern Great Plains during spring, and in the north-central United States, the northern Great Plains, and the Pacific Northwest during summer. In drier climate regions such as the northern Great Plains and north-central United States, soil moisture control on the ESI is confined to surface soil layers, with subsurface soil moisture passively responding to changes in the ESI. The soil moisture–ESI interaction is more uniform between surface and subsurface soils in wetter regions with higher vegetation cover. These results provide a benchmark for simulation of soil moisture–ET coupling and are useful for projection of associated climate processes in the future.

1. Introduction

Soil moisture is a central element of land surface processes by influencing the land energy and water budgets through its impact on evapotranspiration (ET) (Seneviratne et al. 2010). In the classical conceptual framework of three climate regimes (Budyko 1974; Koster et al. 2004, 2019; Seneviratne et al. 2010; Teuling et al. 2009), soil moisture does not impact ET variability in wet and dry climate regimes, but strongly constrains ET variability in a transitional climate regime. Whenever soil moisture decreases limit ET, more energy is available for sensible heat flux, thereby inducing an increase in air temperature (Koster et al. 2006;

Seneviratne et al. 2006a; Gevaert et al. 2018). Increased temperature can lead to a higher vapor pressure deficit and evaporative demand, and thus to an increase in ET and a further decrease in soil moisture. It has been suggested that this positive feedback can go on until the total drying of the soil occurs, intensifying and sustaining drought conditions (Seneviratne et al. 2010). On average this soil moisture–temperature coupling is expected to be stronger in transitional climate regime (Miralles et al. 2012).

As water is needed for photosynthesis and leaf growth, soil moisture impacts plants' productivity and survival during drought. In spring, wet conditions are beneficial to vegetation growth but waterlogged soils can delay planting. Temperatures impact photosynthesis rate, plant and microbial respiration, leaf phenology and

Corresponding author: Yafang Zhong, yafangzhong@wisc.edu

DOI: 10.1175/JHM-D-19-0205.1

© 2020 American Meteorological Society. For information regarding reuse of this content and general copyright information, consult the [AMS Copyright Policy](https://www.ametsoc.org/PUBSReuseLicenses) (www.ametsoc.org/PUBSReuseLicenses).

nutrient release (Myneni et al. 1998; Nadelhoffer et al. 1991; Notaro et al. 2006). Both heat and cold stresses are detrimental to vegetation health because plants' tolerance mechanisms to temperature stresses are effective only in certain thermal ranges (Anderegg et al. 2013; Nievola et al. 2017). In extratropics, both temperature and moisture are main drivers of vegetation activity; whereas in tropics, temperature is arguably less important than water and light. Conversely, vegetation affects soil moisture and temperature mainly through transpiration (Dirmeyer et al. 2006) and albedo feedbacks (Bonan 2002; Teuling and Seneviratne 2008; Lozano-Parra et al. 2018).

Despite the key importance of soil moisture–ET coupling in land–atmosphere interactions, the scarcity of soil moisture and ET observations poses a major impediment for investigation of this coupling regarding spatiotemporal characteristics and possible modifications with climate change (Koster and Suarez 1999, 2001; Dirmeyer 2000; Dirmeyer et al. 2009; Seneviratne et al. 2010). The purpose of this study is to take advantage of a satellite-derived version of the evapotranspiration stress index (ESI; Anderson et al. 2007a,b), as a normalized ratio of actual ET to reference ET, and in situ soil observations from the U.S. Climate Reference Network (USCRN), to better understand and quantify soil moisture–ET coupling and relevant processes. The objective is to explore subseasonal and regional relationships between the ESI and soil moisture, soil temperature, and indirectly, vegetation, across the contiguous United States. Another objective is to examine the relative roles of surface and subsurface soils in the soil moisture coupling with the ESI.

The ESI was introduced in 2007 to the archive of drought indices, with the most widely used indices including the Palmer drought severity index (PDSI; Palmer 1965), the standardized precipitation index (SPI; McKee et al. 1993), and the standardized precipitation and evapotranspiration index (SPEI; Vicente-Serrano et al. 2010). The ESI represents anomalies in the ratio of actual ET to a reference ET that would occur from a well-watered grass surface under optimal meteorological conditions (Mecikalski et al. 2018). Negative ESI anomalies represent smaller-than-normal reference ET fractions for a given location and time of year, indicating higher-than-normal moisture stress in vegetation and thus unhealthy vegetation (Anderson et al. 2007a). As such, the ESI provides useful information about vegetation health and can serve as a drought monitor during agricultural and ecological droughts (Otkin et al. 2015b, 2018). Using satellite data and a fully automated Atmosphere–Land Exchange Inverse model (ALEXI), the ESI maps have been generated

routinely covering the United States (Anderson et al. 2011, 2013). Previous rigorous evaluations of ALEXI over a range of climatic and vegetation conditions have shown that ALEXI ET estimates compare well with ground-based data (Anderson et al. 1997, 2012; Li et al. 2008). The USCRN soil observations have a national coverage and consistent measurement techniques across the United States, with measurements made at multiple soil depths from 5 to 100 cm (Bell et al. 2013). It is worth mentioning that this is not a mechanism study of soil moisture–ET coupling, which may require in situ ET observations such as from the FLUXNET towers (Baldocchi et al. 2001).

This study employs lead–lag correlations to examine the coupling between the ESI and land surface conditions. Due to the complex interactions between soil moisture, ET, temperature and vegetation, it is challenging to tease apart the ESI relationships with soil moisture and temperature in a statistical sense. In our best effort of doing so, partial correlations are used to depict these ESI relationships in addition to regular correlations. Partial correlations find the unique variance between the two variables while eliminating the variance from a third variable, thereby measuring the relationship between two variables while controlling for a third variable. The study also builds upon prior analyses by Notaro et al. (2006) that utilized the covariance of fractional vegetation cover and a lagging air temperature or precipitation metric to quantify the atmospheric responses to changes in vegetation cover for U.S. geographic regions characterized by a similar vegetation type and climatology. The same statistical approach is applied to relate ALEXI ESI to USCRN soil moisture and temperature. The data and methods are described in sections 2 and 3, respectively. Section 4 presents results, with conclusions and discussions provided in section 5.

2. Data

a. Evaporative stress index

In its current formulation, the ESI represents standardized anomalies in the reference ET fraction, ET/ET_{ref} , where ET is the actual ET and ET_{ref} is a reference ET flux that would occur under optimal meteorological conditions from a well-watered grass surface (Anderson et al. 2013). Note that the ratio of actual to reference ET is a bulk crop coefficient. Normalization by reference ET reduces the impact of the non-moisture-related drivers on ET, e.g., the seasonal cycle in solar radiation and evaporative demand. Anderson et al. (2013) has shown that the reference ET fraction exhibits little

seasonal variability in some regions, but considerable seasonality in other areas. To reduce such seasonality, the climatological-mean seasonal cycle is removed from the reference ET fraction before standardization for the time of the year. The reference ET flux is computed using a Penman–Monteith formulation for a well-watered grass (Allen et al. 1998). In its original formulation, the ESI was defined as the ratio of actual ET to a Priestley–Taylor–based estimate of potential ET (Anderson et al. 2007a). However, Anderson et al. (2013) found that reference ET computed from the Penman–Monteith formulation gave better performance.

The actual ET flux is estimated using the ALEXI model (Anderson et al. 2007a, 2011), a regional framework that couples the land surface representation of the Two-Source Energy Balance (TSEB; Norman et al. 1995) model to a simple atmospheric boundary layer model (McNaughton and Spriggs 1986). Using land surface temperatures retrieved from Geostationary Operational Environmental Satellite (GOES) imagery, ALEXI partitions latent and sensible heat fluxes between soil and canopy components of the scene based on the vegetation cover fraction estimates derived from the Moderate Resolution Imaging Spectroradiometer (MODIS) leaf area index product (Myneni et al. 2002). The midmorning surface fluxes are computed for each satellite pixel using the observed increase in land surface temperatures during the morning growing phase of atmospheric boundary layer (from 1.5 h after local sunrise until 1.5 h before local noon). The atmospheric boundary layer model provides closure for the surface energy balance equations, using predawn temperature profiles in the lower troposphere obtained from the Climate Forecast System Reanalysis (CFSR; Saha et al. 2010). Since land surface temperatures are the primary model input, ALEXI diagnoses large surface temperature change as a signature of low ET. ALEXI is run daily over cloud-free pixels on a 4-km-resolution grid covering the contiguous United States.

Because thermal-based satellite retrievals of surface states and fluxes can be hampered by clouds, the daily ET datasets often have limited spatial coverage. To increase the data coverage across the United States, the reference ET fraction is typically composited over a week to multiweek time periods before standardization (Hain et al. 2009; Otkin et al. 2014, 2015a). ESI, expressed as pseudo z scores normalized to a mean of 0 and a standard deviation of 1, is computed for each week using these composites of reference ET fraction. This study uses weekly 7-day composite ESI values, with the mean and standard deviations for each week computed separately for each grid point using data from 2001 to 2017. Weekly ESI was generated for each

USCRN site using the averages across the nine grid points centered on the grid point nearest to the USCRN station. The use of 3×3 grid aggregation increases the sample size, thereby reducing impacts of noise.

b. USCRN soil data

The soil moisture and temperature measurements by the USCRN commenced in 2009 to 2010 (Bell et al. 2013). The USCRN sites differ vastly in terms of soil, climate, and vegetation conditions (Wilson et al. 2016). For each site where the soil profile allows, soil measurements are made at five depths: 5, 10, 20, 50, and 100 cm. This study includes data from sites that offer at least 7 years of soil moisture data from the 5 cm depth during the time period from 2010 to 2017 (Fig. 1). When the subhourly raw data are flagged as erroneous, the corresponding daily data are reported as missing.

In this study, the soil information has been condensed into three soil layers (0–20, 50 and 100 cm) to simplify discussion. To estimate the average conditions for the topsoil layer above 20-cm depth, the daily soil data are linearly interpolated to a 1-cm resolution depth ordinate. First, the measurement values are assigned to corresponding depths of the new depth ordinate, with the top 5 cm adopting values from measurements at 5-cm depth. Second, linear interpolation is used to fill in missing values, with the missing beginning and end points remain as they were (<https://www.ncl.ucar.edu/Document/Functions/Built-in/linmsg.shtml>). Third, if over half of the resultant soil moisture or temperature data in the 0–20-cm layer have nonmissing values, then averages were taken across the vertical profiles in the upper 20 cm to depict soil conditions for the new topsoil layer. Hereafter, discussions of soil moisture and temperature conditions are referred to as topsoil (0–20 cm), subsoil (50 cm), and deep soil layers (100 cm). As for the ESI, daily averages of soil moisture and temperature data are composited into weekly values. With the removal of the mean seasonal cycle between 2010 and 2017, weekly ESI, moisture and temperature anomalies are derived and used in further analyses.

3. Methods

a. Regional analysis

Because the USCRN soil records are rather short in time, regional analysis is applied to obtain more robust results. The seven geographic regions (Fig. 1) considered are the Pacific Northwest (PNW), southwestern United States (SWUS), northern Great Plains (NGP), southern Great Plains (SGP), north-central United

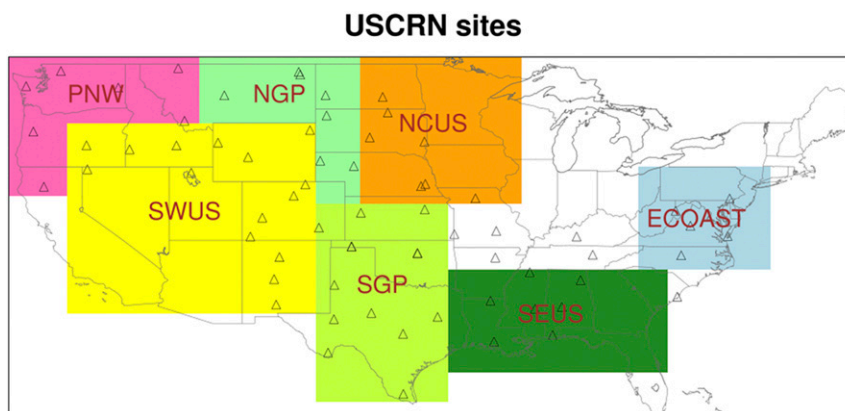


FIG. 1. A map shows the USCRN sites that offer at least 7 years of data for 5-cm soil moisture during the time period of 2010–17. Color blocks outline the seven regions each characterized by a same vegetation type.

States (NCUS), southeastern United States (SEUS), and East Coast of United States (ECOAST), with each region characterized by a similar climatology and vegetation type. The outlines of the regions are approximate to those used in the regional analysis by [Notaro et al. \(2006\)](#) that examined the impacts of fractional vegetation cover on air temperature and precipitation. Each of the regions contains 5–15 selected USCRN sites, with the largest amount of weekly data for the SGP and SWUS and least for the ECOAST and PNW ([Fig. 2](#)). In general, the topsoil layer offers more samples than the subsoil and deep soil layers, and more samples are available for soil temperature than for soil moisture. For all of the variables, regions, and calendar months during the growing seasons, a Pearson correlation greater than 0.14 in magnitude is statistically significant at $\alpha = 0.05$ according to a two-tailed t test.

b. Contemporaneous correlation analysis

Contemporaneous correlation analysis is a common technique in the study of land–atmosphere coupling, and the temporal correlation between soil moisture and ET has been used as a standard metric for evaluating the coupling strength ([Dirmeyer et al. 2009](#); [Lei et al. 2018](#)). A positive correlation represents the control of soil moisture on ET in a soil moisture-limiting regime. A negative correlation indicates soil moisture responds to ET forcing rather than controlling ET in an energy-limiting regime ([Dirmeyer 2011](#)). This clear-cut difference makes contemporaneous correlation a powerful tool in depicting the coupling between soil moisture and ET. Here, Pearson correlations are computed between soil moisture, soil temperature, and the ESI for the growing season and for each of the seven regions, using weekly anomalies between March and October during

the time period of 2010–17 and from all of the selected sites in that region. However, the contemporaneous correlation between soil moisture and the ESI offers a more complex picture due to the inclusion of a third player in reference ET. A positive correlation between soil moisture and the ESI may result from soil moisture control on ET or result from elevated moisture stress (i.e., negative ESI and worse-than-average moisture availability) due to increased evaporative demand. The contemporaneous correlation is thus not very effective at depicting the coupling between soil moisture and the ESI; however, this issue can be remedied through use of lead–lag correlation analysis, as discussed in the next section.

c. Lead–lag correlation analysis

Lead–lag correlation analysis is widely used in the study of ocean–atmosphere coupling to help identify the driving mechanisms. For example, the largely symmetric correlations of monthly wind and sea surface temperature (SST) with respect to the lags indicate essentially two-way interactions in the tropics ([Lian et al. 2018](#)); whereas in the extratropics, the much heavier loading at wind-leading-SST lags indicates the surface wind is driving the SST primarily ([Frankignoul and Hasselmann 1977](#); [Zhong and Liu 2009](#)). Similarly, this study uses lead–lag correlation analysis to qualitatively describe the relationship between the ESI and land surface conditions over subseasonal time scales. The lead–lag correlations are also used to evaluate the seasonal memory of the ESI, soil moisture, and soil temperature. The length of memory conveys information about the impact of land surface conditions on the ESI as well as the suitability of the generalized equilibrium feedback assessment (GEFA) for this study (refer to [section 3f](#)). The longer the memory the ESI exhibits, the stronger

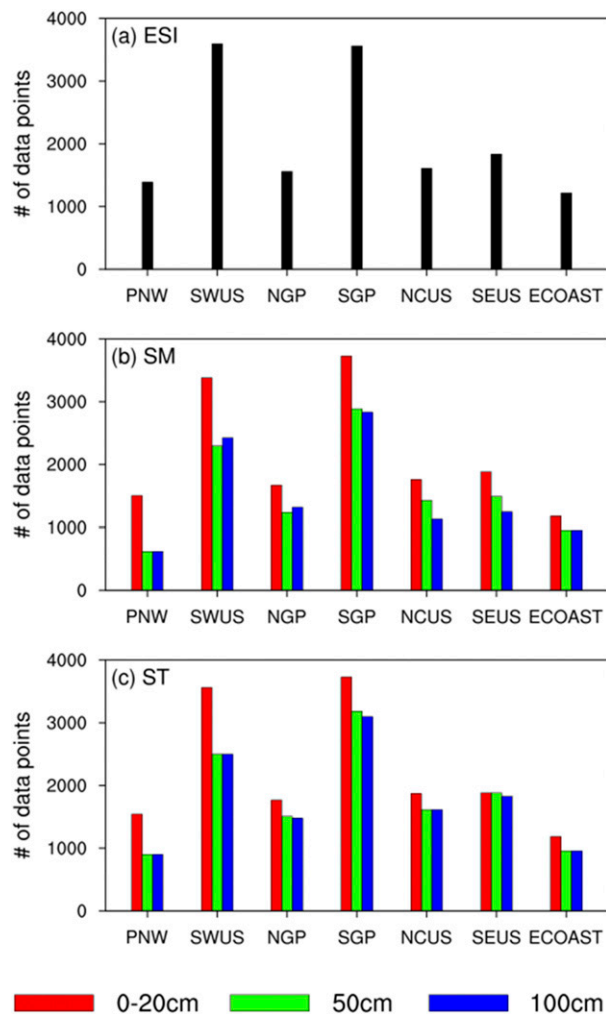


FIG. 2. Bar charts show the data volume (weeks) for each of the seven regions and three soil layers during March–October between 2010 and 2017: (a) ESI, (b) USCRN soil moisture (SM), and (c) USCRN soil temperature (ST).

influence the land surface conditions exert on the ESI. By formulation, the GEFA method requires fast-changing fields as the response fields and slow-changing fields as the forcing fields, with sufficient separation in memory between them.

d. Partial correlation analysis

In recognition of the generally negative relationship between soil moisture and soil temperature that presumably stems from soil moisture–temperature coupling, partial correlation analysis is used to discriminate the impact of soil moisture from that of soil temperature on the ESI. A partial correlation coefficient describes the strength of a linear relationship between two variables, holding constant a third variable (Freund et al. 2010). For example, the partial correlation coefficient

for the ESI and soil moisture, controlling for soil temperature, can be formulated as

$$r_{EM,T} = \frac{r_{EM} - (r_{TE})(r_{TM})}{\sqrt{1 - r_{TE}^2} \sqrt{1 - r_{TM}^2}}, \quad (1)$$

where r_{EM} is Pearson correlation coefficient between ESI and soil moisture, r_{TE} is that between soil temperature and ESI, and r_{TM} is that between soil temperature and soil moisture. Given the complex relationships between ET, soil moisture, and temperature as discussed in the introduction, partial correlation analysis is superior to regular correlation analysis because it can separate the impacts of soil moisture and soil temperature on the ESI. However, partial correlation analysis may increase uncertainty in correlation coefficients where there are very strong relationships between soil moisture and soil temperature. Multicollinearity problems arise when the correlations between soil moisture and soil temperature approach -1 , and it becomes difficult to separate out effects of one of the variables.

Partial correlations are computed for each calendar month between March and October and for each of the seven regions using weekly ESI anomalies from that region and the specified month during the time period of 2010–17, and weekly soil moisture and soil temperature anomalies from previous weeks or subsequent weeks. For instances, correlations for June at lag -1 are computed using weekly ESI anomalies from the 22nd, 23rd, 24th, and 25th weeks of the year, and weekly soil anomalies from the 21st, 22nd, 23rd, and 24th weeks of the year; correlations for June and lag $+1$ are computed using weekly ESI anomalies from the 22nd, 23rd, 24th, and 25th weeks of the year, and weekly soil anomalies from the 23rd, 24th, 25th, and 26th weeks of the year. Weekly anomalies from all of the selected sites in that region and from the consecutive four (or five) weeks between 2010 and 2017 are aggregated before the computation of partial correlations with Eq. (1). Partial correlations are computed from lag -12 to $+12$. If the ESI is missing due to being out of season, the weekly anomalies are set to missing and ignored in the computation of partial correlations.

Monte Carlo tests are performed to determine if the partial correlations are statistically significant at $\alpha = 0.05$ (von Storch and Zwiers 1999; Czaja and Frankignoul 2002). Again, using June and lag -1 as an example, weekly ESI anomalies from the 22nd, 23rd, 24th, and 25th weeks of the year are reshuffled randomly between years and the resultant new time series are used to compute the partial correlations with soil moisture and soil temperature from the 21st, 22nd, 23rd, and 24th weeks of the year. Note that only the order of the years for ESI anomalies is changed,

not that of the weeks or the sites, so that the autocorrelation of ESI anomalies at lags from 1 to 12 weeks and the spatial correlation are unchanged. By doing so, the impact of temporal and spatial correlations within each variable on the effective sample size for estimating the partial correlations is taken into account in the Monte Carlo tests. This procedure is repeated 1000 times. If the original partial correlation with soil moisture or soil temperature is greater in strength than 95% of the corresponding 1000 new values, then that partial correlation is considered statistically significant. The significance of the partial correlations is not shown for the clarity on the figures, but has been used to determine if the ESI responses to land surface forcing are statistically significant as described in section 3f.

e. Calculation of seasonal memory

The memory in the ESI and the seasonality for each of the seven regions are evaluated with lead-lag correlation analysis. Similar to the calculation of partial correlations, Pearson correlations are computed for each calendar month and from lag -40 to $+40$, using weekly ESI anomalies from the specified region and month during the time period of 2010–17, and those from previous weeks or subsequent weeks. Based on these correlations, a decorrelation time is estimated for each month and both for the negative lags and for the positive lags using the critical correlation of $+0.14$. The average of the decorrelation times from the negative lags and from the positive lags is determined as the ESI memory as a function of calendar month. Similarly, the seasonal memory is estimated for soil moisture and soil temperature for all three of the soil layers.

f. Generalized equilibrium feedback assessment

While the lead-lag partial correlations can help determine whether the relationships between the ESI and land surface conditions are one-way or two-way coupling, the GEFA method is used to more quantitatively assess the impact of land surface conditions on the ESI. The response coefficients estimated by the GEFA quantify the instantaneous response of the ESI to changes in land surface conditions. The GEFA method was originally developed by Liu et al. (2008) as a generalization of the univariate equilibrium feedback assessment (EFA; Frankignoul et al. 1998; Notaro et al. 2006) to facilitate distinguishing the impacts on the atmosphere and surface fluxes from persistent and also interrelated oceanic forcings (Liu and Wen 2008; Zhong et al. 2011). The key difference between this approach and Granger causality based on the notion of predictability (Salvucci et al. 2002; Sugihara et al. 2012; Tuttle and Salvucci 2017) is that the former uses

response coefficients to quantify the instantaneous changes in the atmosphere (and/or surface fluxes) under the land forcing (Liu et al. 2006; Notaro et al. 2006), whereas the latter allows identifying the causality between the land and the atmosphere at a later time. For instance, Kaufmann et al. (2003) applied Granger causality to quantify the lagged temperature response to interannual changes in vegetation. The instantaneous response would be greater than the lagged causality response, as the difference representing the decay of the forcing with time (Liu et al. 2006; Notaro et al. 2006). The formulation of the GEFA is briefly summarized here.

Assume that the surface flux variability, such as the ESI variability $\mathbf{E}(t)$, consists of a stochastic part associated with the atmospheric internal variability $\mathbf{N}(t)$ and a land surface condition-forced part $\mathbf{B} \times \mathbf{S}(t)$, such that

$$\mathbf{E}(t) = \mathbf{B} \times \mathbf{S}(t) + \mathbf{N}(t). \quad (2)$$

The land surface field $\mathbf{S}(t)$ consists of J forcings, representing J land surface variables. The term \mathbf{B} is the response sensitivity vector with elements b_j measuring the impact of the j th land surface variable on the ESI. Using data with the ESI lagging the land surface conditions (Frankignoul et al. 1998; Czaja and Frankignoul 2002), \mathbf{B} is derived from the ESI-lagged covariances as

$$\mathbf{B}(\tau) = \mathbf{C}_{\text{ES}}(\tau)\mathbf{C}_{\text{SS}}^{-1}(\tau), \quad (3)$$

where τ is an ESI lag time that is longer than the damping time scale of the atmosphere, $\mathbf{C}_{\text{ES}}(\tau)$ is the lagged cross-covariance vector between the ESI and land surface conditions, and $\mathbf{C}_{\text{SS}}(\tau)$ is the autocovariance matrix of land surface conditions. Here, the land surface field consists of two variables, soil moisture and soil temperature. This is a simplification of the land surface forcing since vegetation is not included explicitly.

As for the partial correlation coefficients, the lagged cross-covariance vector and the autocovariance matrix are estimated for each of the seven regions and for each calendar month between March and October. Response coefficients in \mathbf{B} are then computed with Eq. (3), representing the changes in the ESI due to a change in weekly soil moisture or soil temperature. This procedure is performed for each lag between 5 and 8 weeks and the final GEFA response is the averaged results from the four lags. To determine if the response coefficients are statistically significant at $\alpha = 0.05$, Monte Carlo tests are performed with the ESI data reshuffled 100 times. Further screening of the significant responses is made by requiring that the corresponding partial correlation

coefficients from the four lags share the same sign, in that variations in the signs of these partial correlation coefficients could signify transient soil anomalies but the formulation of the GEFA method assumes a persistent forcing on the atmosphere. For instance, for the ESI response to soil moisture during June to be considered as a significant response, the partial correlations between the ESI and soil moisture at the ESI lagging by 5–8 weeks must all be positive or negative.

4. Results

The regional and seasonal relationships of the ESI to soil moisture and temperature were assessed using contemporaneous correlation analysis, lagged partial correlation analysis and the GEFA method, first to provide a brief overview of the relationships during the growing seasons and then to elaborate on those relationships.

a. Relationships between the ESI, soil moisture, and soil temperature

This subsection provides an overview of the regional relationships between the ESI, soil moisture and soil temperature during the growing seasons between March and October based on contemporaneous correlations. Correlations greater than 0.14 in magnitude are statistically significant at $\alpha = 0.05$. Because the relationships between the variables intrinsically depend on moisture regimes and are typically nonlinear as the season progresses (Koster et al. 2009), linear correlations should be viewed as a simplification of the relationships.

For all regions except the ECOAST, the ESI is positively correlated with soil moisture for each of the three soil layers, with the highest correlations from the topsoil layer (Fig. 3a). These positive correlations could reflect soil moisture control on ET, or elevated moisture stress due to enhanced evaporative demand. The correlations from the topsoil layer are largest for the SGP (+0.49) and smallest for the ECOAST (<+0.15), agreeing with the findings of Otkin et al. (2018) based on gridded maps of contemporaneous correlations between the ESI and modeled soil moisture anomalies from the North American Land Data Assimilation System Phase 2 (NLDAS-2; Xia et al. 2012 a,b). The correlations are smaller in the eastern United States as it lies in an energy-limiting regime most of the year. In the SGP and PNW, the correlations from the subsoil and deep soil layers are close to those for the topsoil layer, indicating a tight moisture coupling between the layers. In the SWUS, NGP and NCUS, however, the correlations decrease markedly for the deeper layers compared to the topsoil layer. The decrease occurs at a

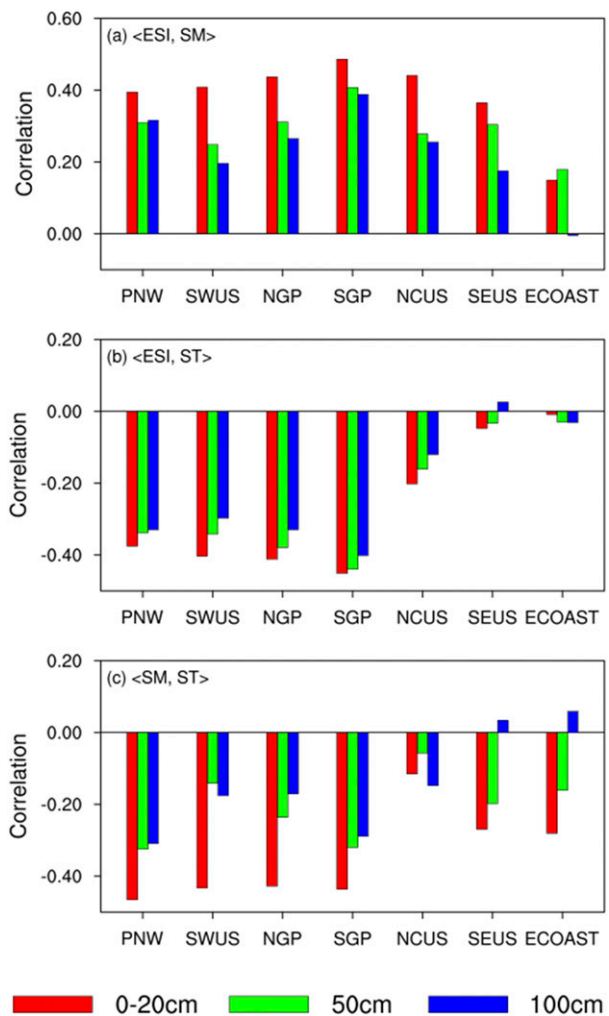


FIG. 3. Bar charts show temporal correlations between weekly ESI and USCRN soil properties for the seven regions and three soil layers during March–October between 2010 and 2017: (a) between ESI and soil moisture (SM), (b) between ESI and soil temperature (ST), and (c) between SM and ST.

greater depth in the SEUS as the correlations for the subsoil layer remain close to those for the topsoil layer. It appears that the subsoil and deep layers play an active role in the soil moisture–ET coupling in relatively wet climate regions, consistent with the finding of Short Gianotti et al. (2019) that wet areas tend to exhibit stronger surface–subsurface moisture coupling.

The ESI is negatively correlated with soil temperature in the western and central United States (Fig. 3b), and not correlated in the eastern United States. The negative correlations reflect the fact that the thermal-based ALEXI model diagnoses high surface temperature as a signature of low ET, and there is likely correlation between surface temperature and subsoil temperatures. The correlations are marginally stronger for the

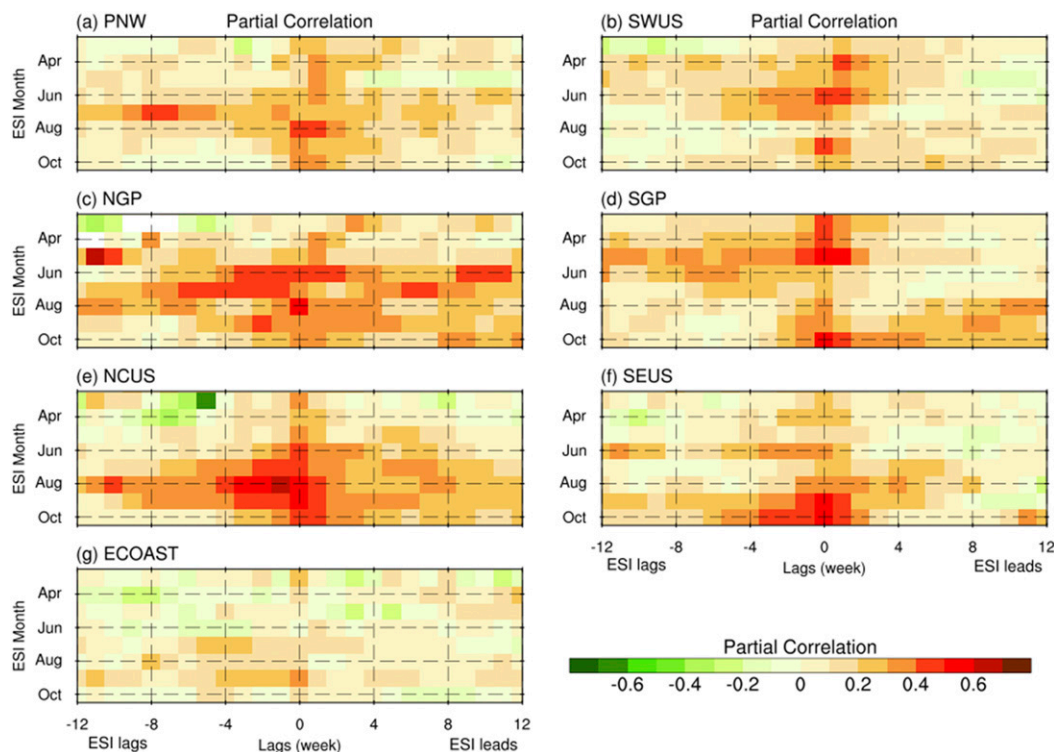


FIG. 4. Lead-lag partial correlations between the ESI and topsoil moisture (0–20 cm) from the USCRN measurements for the time period of 2010–17: (a) PNW, (b) SWUS, (c) NGP, (d) SGP, (e) NCUS, (f) SEUS, and (g) ECOAST. The y coordinate denotes the ESI in a specified calendar month between March and October, and the x coordinate denotes the ESI leading or lagging soil moisture by up to 12 weeks.

topsoil layer than the subsoil and deep soil layers, and strongest for the SGP and weakest for the NCUS. The correlations between soil moisture and soil temperature are generally negative, with the strongest correlations (< -0.30) found for the topsoil layer of the western United States and the Great Plains as well as the subsoil and deep soil layers of the SGP and PNW (Fig. 3c). Overall, the correlations between the ESI and soil moisture and soil temperature are strongest for the western and central United States due to soil moisture–ET coupling and soil moisture–temperature coupling (Seneviratne et al. 2010). The ESI correlations are stronger with soil moisture and temperature in the topsoil layer than in the subsoil and deep soil layers.

b. Coupling between the ESI and land surface conditions

The relationships between the ESI anomalies and changes in soil moisture and temperature are explored using the lead-lag partial correlation analysis. Figures 4 and 5 display the partial correlations with soil moisture and soil temperature from the topsoil layer both for the ESI lagging and the ESI leading by up to 12 weeks. The

impacts of land surface conditions on the ESI can be inferred from the partial correlations with the ESI lagging, while the utility of the ESI as an indicator of subsequent land surface conditions is reflected in the partial correlations with the ESI leading. The calendar months in the y coordinate refer to the time period used to compute the ESI.

The partial correlations with topsoil moisture are generally positive throughout the growing season across the United States, both for the ESI lagging and for the ESI leading. The partial correlations with topsoil temperature are weaker and rather noisy as a whole. In the SGP, known as a hot spot for land–atmosphere coupling, the partial correlations with topsoil moisture are stronger at the ESI lagging than at the ESI leading during April–June (Fig. 4d), indicating the control of topsoil moisture over the ESI. Note that the seasons are referred to the time period used to compute the ESI. This helps explain the strong ESI–soil moisture coupling during spring as evidenced by the large partial correlations (+0.55) at lag 0. During July–September, the ESI is moderately correlated with topsoil moisture as well as topsoil temperature as a proxy for surface temperature (Fig. 5d). In October, the ESI is strongly coupled with

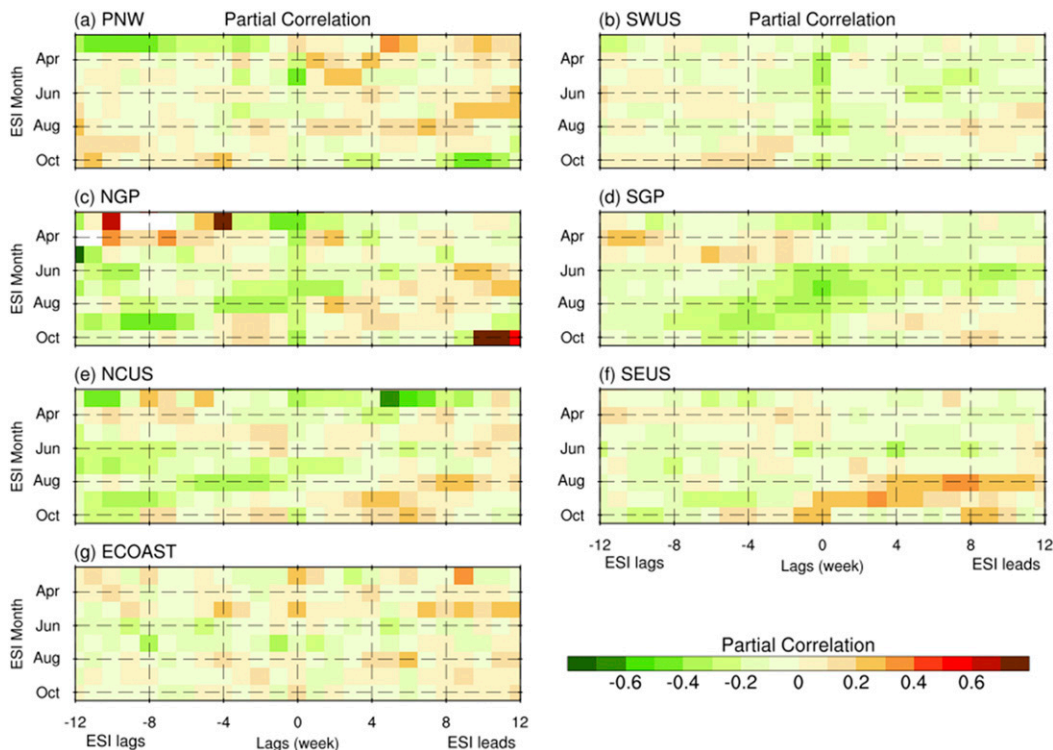


FIG. 5. As in Fig. 4, but for lead-lag partial correlations between the ESI and topsoil temperature.

topsoil moisture and is also a good indicator of subsequent moisture availability (Fig. 4d).

The strongest evidence for soil moisture control over the ESI is found in the NCUS, where the partial correlations between the summertime ESI and topsoil moisture from the preceding weeks are as high as $\sim +0.50$ (Fig. 4e). Such control of topsoil moisture on the ESI is also significant in the NGP and PNW during July. On the other hand, the relationship of the ESI to subsequent topsoil moisture is strongest in the NGP during summer, with seasons referred to the topsoil moisture. The relationship of the ESI to subsequent topsoil temperature can go opposite ways (Fig. 5). The cooling effect of ET can result in a negative partial correlation between the ESI and topsoil temperature, as can the changes in evaporative demand under heat waves, e.g., in the SGP during summer. Positive correlations between the ESI and subsequent topsoil temperature are found in the SEUS and NCUS during late summer and early fall.

Lead-lag partial correlations are also computed using soil data from the subsoil and deep soil layers. The seasonal patterns of the partial correlations are similar to those from the topsoil layer for all regions except the NGP and NCUS. For these two regions, compared to those with topsoil moisture, the partial correlations with

deeper soil moisture tend to shift the loading from the ESI lagging side toward the ESI leading side during summer and fall, with seasons referred to the time period used to compute the ESI (Figs. 6 and 7). This indicates a more passive role by the soil moisture of deeper layers in the interactions with the ESI over sub-seasonal time scales, because of bare soils or shallow-rooted vegetation. Compared to topsoil temperature, the deeper soil temperature exhibits more negative partial correlations, particularly during summer at the ESI lagging. The strong correlations between July ESI and April deep soil temperature may be attributed to the lingering effect from snow cover.

These results accentuate the complex relationships between the ESI and soil conditions that exhibit strong seasonality and regional characteristics. The ESI is most strongly coupled with soil moisture (partial correlations > 0.40) in the SGP during April–May and October, in the NGP during June–July, in the NCUS from June to October, in the PNW during July–August and October, in the SWUS during April–July and September, and in the SEUS during September–October. Here, seasons are referred to the time period used to compute the ESI. The strong coupling in the SGP during spring, in the NGP and PNW during July, and in the NCUS during June–September stems from

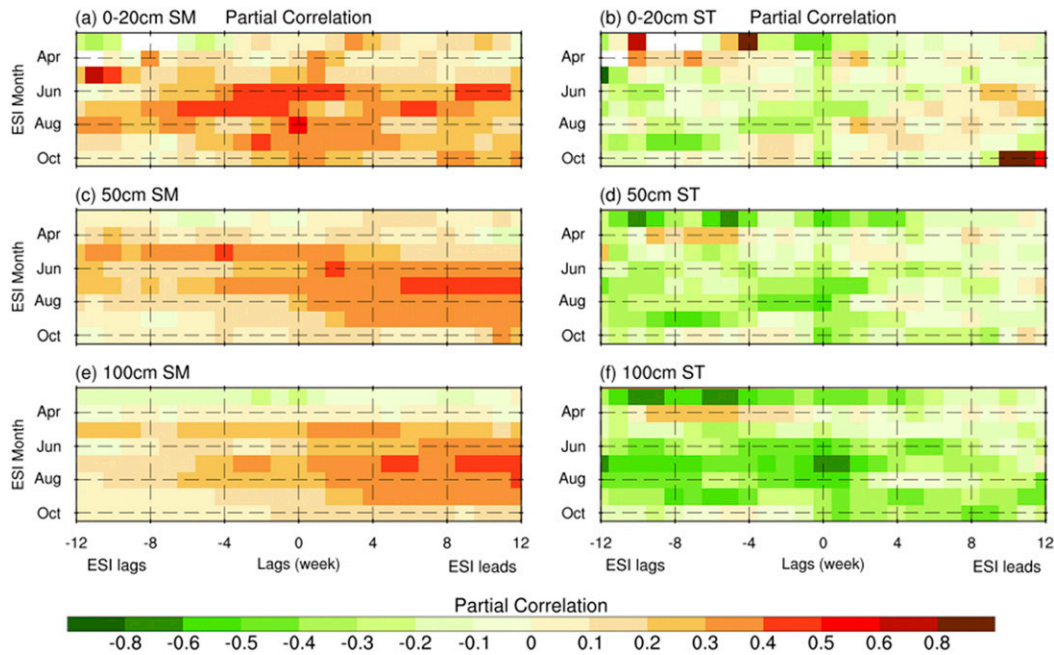


FIG. 6. Lead-lag partial correlations between the ESI and (left) soil moisture and (right) soil temperature for the northern Great Plains (NGP) using the USCRN measurements at (a),(b) 0–20, (c),(d) 50, and (e),(f) 100 cm for the time period of 2010–17. The y coordinate denotes the ESI in a specified calendar month between March and October, and the x coordinate denotes the ESI leading or lagging soil moisture by up to 12 weeks.

the control of soil moisture on the ESI as manifested by the greater correlations at the ESI lagging than ESI leading. In the NGP and NCUS, the summertime ESI could be a good indicator of subsequent soil moisture in deeper layers. The

ESI is also tightly coupled with deeper soil temperature (partial correlations < -0.40) in the SGP and NGP from June to October, and in the NCUS during June–July. The strong correlations in the NGP and NCUS at the ESI

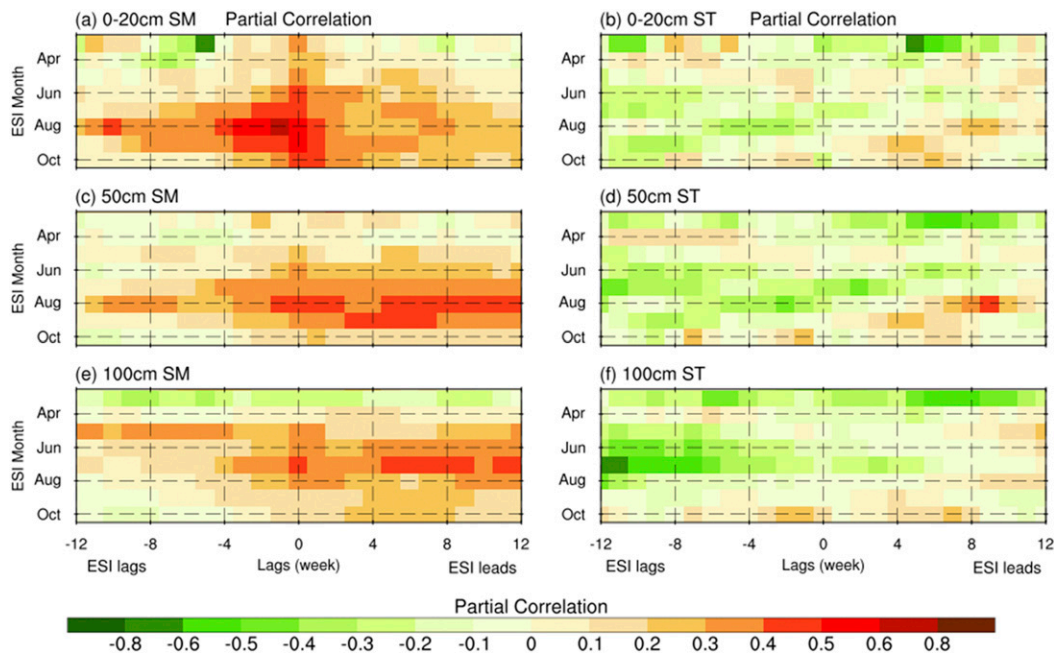


FIG. 7. As in Fig. 6, but for the north-central United States (NCUS).

lagging suggest that information about deep soil temperature could be exploited to predict the ESI over subseasonal time scales.

c. Quantifying the impacts of soil conditions on the ESI

Numerous studies have evaluated the coupling strength of soil moisture and surface fluxes and variables (e.g., ET and air temperature) using either observations (e.g., Mueller and Seneviratne 2012; Lei et al. 2018) or model simulations (e.g., Koster et al. 2006; Dirmeyer 2011), but they rarely attempt to separate the control of soil moisture on ET and temperature from that of ET and temperature on soil moisture. Here, the influence of land surface processes on the ESI is assessed with the memory (or persistent time) of the ESI anomalies. The memory of the ESI varies greatly with season and region, ranging from less than a week to up to 17 weeks (Fig. 8a). Since the persistence time of synoptic meteorological conditions is less than a couple of weeks, an ESI memory longer than that indicates influence from land surface conditions. The longest memory (>8 weeks) in the ESI is found in the central United States from June through September, indicative of strong coupling with land surface processes such as depletion of soil moisture and vegetation phenology. The land surface influence on the ESI is also shown in the SWUS during spring and in the SEUS from midsummer to early fall.

The soil moisture and temperature memories are much longer (Figs. 8b,c), typically ranging between 6 and 30 weeks. As expected, deeper soils generally have longer memory than the topsoil layer, with the latter more directly exposed to synoptic meteorology. In rare occasions, the soil moisture memory of topsoil layer could be longer than that of subsoil and deep soil layers due to snow cover and other processes at high elevations (e.g., in the PNW) (Fig. 8b). Soil moisture exhibits relatively short memory in the topsoil layer of the eastern United States and SWUS compared to locations in the central United States, which is consistent with the finding of Seneviratne et al. (2006b) that soil moisture memory from multimodel simulations is highest at intermediate soil wetness. It may be because precipitation plays a dominant role for the variations in moisture in the former regions, whereas the coupling with ET gets more important in the latter region (Koster et al. 2019). Topsoil temperature exhibits relatively long memory in the SGP and SEUS during most of the growing season, and in the NGP and NCUS during spring and early summer, indicating a role of soil moisture–temperature coupling and vegetation dynamics.

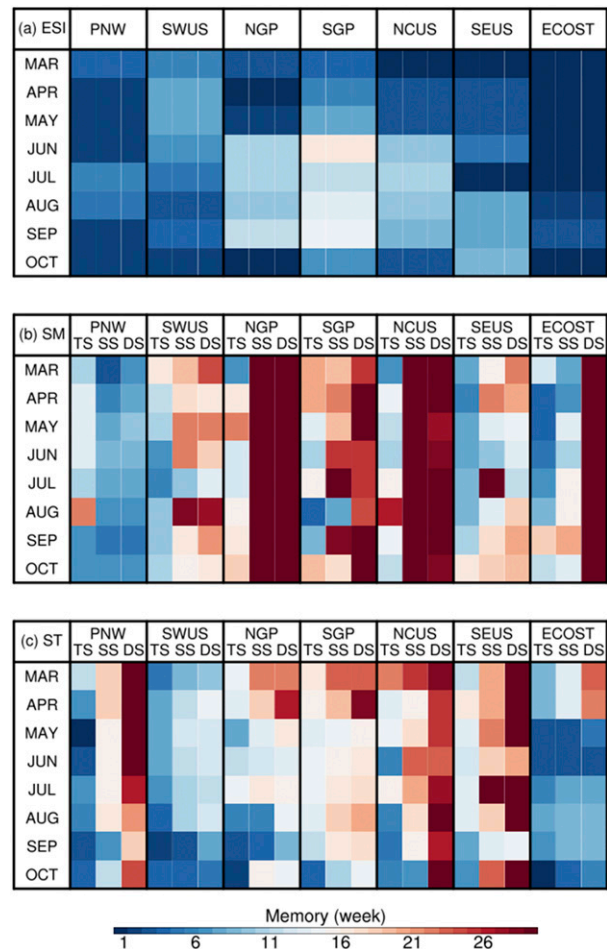


FIG. 8. Seasonal memory (weeks) in (a) the ESI, (b) soil moisture (SM), and (c) soil temperature (ST) as estimated with lead-lag correlations for the seven regions and three soil layers. TS, SS, and DS denote topsoils, subsoils, and deep soils, respectively.

Instantaneous ESI responses to changes in soil moisture and to changes in temperature are quantified with the GEFA method. The GEFA is applied to the ESI response field and to each of the land surface forcing fields. Since topsoil and subsoil moisture and temperature occasionally have a relatively short memory (<6 weeks), the soil data from the deep soil layer are used to best ensure sufficient separation from the ESI in memory while serving as a surrogate for the columnar soil conditions. That is, the ESI responses are not attributed to changes in the deep soil layer solely, but to changes in the entire soil column more likely. The GEFA results suggest that the ESI responds positively to changes in soil moisture mostly and negatively to changes in soil temperature (Fig. 9), in agreement with the results based on the ESI-lagging partial correlations. Note that only significant ESI responses are shown here. The negative responses to soil moisture in the NCUS

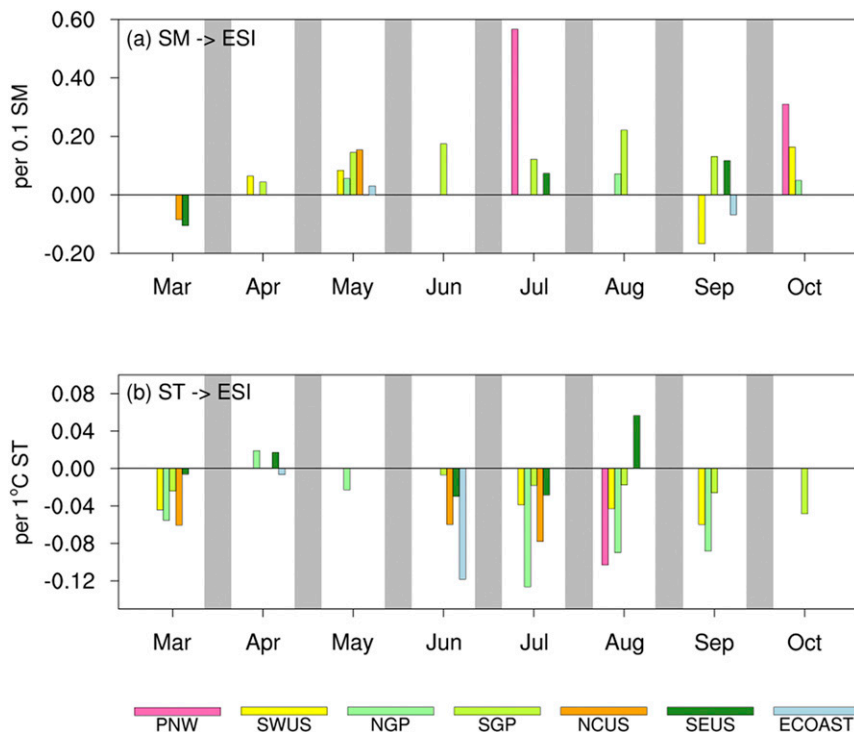


FIG. 9. Monthly mean ESI responses to changes in (a) soil moisture (per 0.1 SM) and (b) soil temperature (per 1°C ST) as estimated with the GEFA method and 100-cm soil data for the seven regions.

and SEUS during March are likely related to snow cover and delay of planting in waterlogged soils; and those in the ECOAST during September may result from the detrimental impacts of hurricanes on vegetation (Fig. 9a). The positive responses to soil temperature in the NGP and SEUS during April likely represent early green-up in warm springs (Fig. 9b).

In the SGP, the ESI responds significantly both to changes in soil moisture and to changes in soil temperature as a proxy for surface temperature during most of the growing season. The fraction of the ESI variability explained by soil moisture variability is higher in spring than in summer, as discussed above with partial correlations. The partial correlation analysis identifies topsoil moisture control of summertime ESI in the NCUS, NGP, and PNW, but the GEFA captures that in the PNW only, perhaps due to the use of deep soil moisture as the forcing field and the potential decoupling from topsoil moisture. For comparison, the hot spots of summertime land–atmosphere coupling in the North America revealed by a multimodel estimate included the SGP, NGP, and PNW (Koster et al. 2004). The significant ESI responses to changes in soil temperature during June–September confirm that surface temperature is a good indicator of vegetation health across the United States in summer (Karnieli et al. 2010).

The scatterplot of the significant ESI responses to changes in soil moisture versus the background soil moisture displays generally positive responses in drier climate regimes and a first-order inverse relationship with background soil moisture (Fig. 10). The inverse relationship is consistent with the various functionals that have been proposed to approximate the dependence of ET on soil moisture (Jarvis 1976; Campbell and Norman 1998; Chen and Dudhia 2001; Hain et al. 2009). In wetter regimes, the ESI responses could be positive or negative, showing no clear tendency with background soil moisture increasing. This agrees with the finding of Dirmeyer et al. (2000) and Koster et al. (2004) that ET in wet climates is not highly sensitive to soil moisture variations.

5. Conclusions and discussion

This study explores the spatiotemporal characteristics of the ESI coupling with soil moisture and relevant processes, as well as the relative roles of surface and subsurface soils in the coupling. The lead–lag partial correlations reveal strong seasonality and regional characteristics of the ESI–land surface interactions across the United States. The control of soil moisture on the ESI is strongest in the SGP during spring, and in

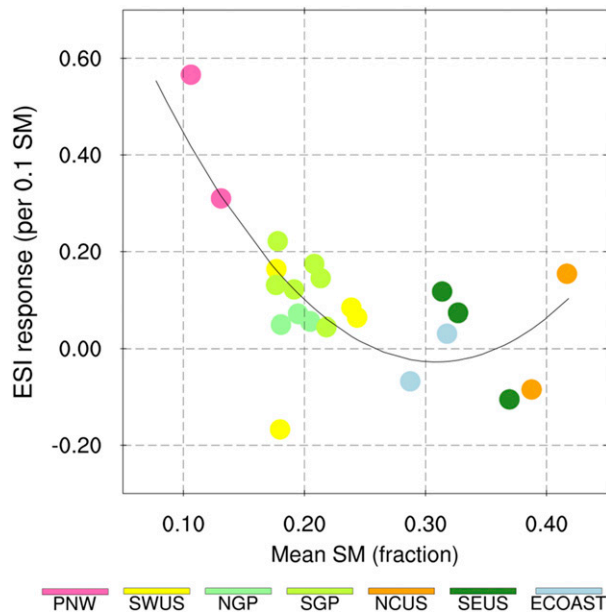


FIG. 10. Scatterplot of the ESI responses to soil moisture (per 0.1 SM) from Fig. 9a vs background soil moisture. The black curve represents the second-degree polynomial determined by a least squares fit to the data.

the NCUS, NGP and PNW during summer, as evidenced by the relatively large positive partial correlations at the ESI lagging. In wet climate regions, the subsoil and deep soil layers tend to act in synergy with the topsoil layer regarding soil moisture coupling with the ESI; whereas in relatively dry regions such as the NCUS and NGP, they are not actively involved. Soil temperature as a proxy of surface temperature exhibits strong negative correlations at the ESI lagging in the NGP and NCUS during summer. It indicates the control of vegetation dynamics on the ESI, as surface temperature tends to negatively relate to vegetation health in a moisture-limiting regime.

The GEFA estimates of ESI responses to deep soil moisture and temperature are able to confirm a significant dependency of the ESI on soil moisture or temperature in these instances of land surface control of the ESI, given that the deep soil moisture and temperature well represent the columnar soil conditions. The significant ESI responses to soil moisture across the contiguous United States conform to a first-order inverse relationship with background soil moisture in drier climate regimes; whereas in wetter regimes, the ESI responses are not obviously related to background soil moisture. Even though the details of the ESI–soil moisture relationship often depend on soil and vegetation properties (Dirmeyer et al. 2000, 2009; Hain et al. 2009), our results suggest that such a pattern is a

general rule across vegetation types and the typical range of soil moisture. The GEFA estimates provide a more integrated assessment of the land surface influence on the ESI than the lead–lag partial correlations, and can be readily used as a coupling metric to facilitate model–observation comparisons.

This work aims to document the spatiotemporal characteristics of the ESI coupling with soil moisture, rather than to deepen the understanding of land–atmosphere interactions. Since remotely sensed surface temperature is a primary input to the ALEXI model, we caution against inferring a causal relationship between the ESI and soil moisture and temperature from the results presented. That being said, these results are still relevant for the study of land–atmosphere interactions as ALEXI ESI is a satellite-derived dataset and has been shown to compare well with ground-based data.

Soil moisture and temperature measurements from the USCRN are used in the partial correlation analysis and GEFA assessment to represent the land surface forcing on the ESI. These are point-scale measurements with correlation lengths for soil moisture fields typically ranging from 10 m to 1 km (Grayson and Western 1998). However, due to the static influence of soil, vegetation, and topography, surface soil moisture fields exhibit temporally persistent spatial patterns at local scales up to 5 km (Jacobs et al. 2004; Crow et al. 2005). The partial correlations and GEFA responses thus depict the relationship between the finescale ESI (~ 12 km, from 3×3 grid aggregation) and local-scale soil moisture patterns. Note that moisture fields in adjacent soils are also interacting with the ESI, which is not captured due to the spatially limited representation of in situ measurements. Indeed, the spatial representation of in situ soil moisture measurements is a long-standing issue for soil moisture observations and the applications in the study of land–atmosphere interactions. Continuing efforts have been devoted to selecting measurement sites that represent a wider geographic area, upscaling of soil moisture measurements, and evaluating spatial representativeness of existing soil moisture data, among others (Mohanty and Skaggs 2001; Crow et al. 2005; Ford and Quiring 2019).

The USCRN network offers limited number of measurement sites that meet the selection criterion of this study, with only a handful of sites in the ECOAST. For future work, we will include other networks from the National Soil Moisture Network to increase data amount. For example, Soil Climate Analysis Network (SCAN) measures soil moisture and temperature at the same five depths as the USCRN, and has a national coverage as well. Similar analyses may also be applied to

in situ ET observations from the FLUXNET towers. Our initial survey of FLUXNET ET and soil data shows good data availability in the SWUS and NCUS, but poor in the other regions.

Acknowledgments. This work is supported by the NOAA Climate Program Office (CPO) Sectoral Applications Research Program (SARP) under Grant NA16OAR4310130. Discussions with Dr. Michael Notaro helped in the explanation of the results. Constructive and thorough comments from the reviewers also improved the manuscript.

REFERENCES

- Allen, R. G., L. S. Pereira, D. Raes, and M. Smith, 1998: Crop evapotranspiration: Guidelines for computing crop water requirements. FAO Irrigation and Drainage Paper, 56, 300 pp., www.fao.org/docrep/X0490E/X0490E00.htm.
- Anderegg, W. R. L., J. M. Kane, and L. D. L. Anderegg, 2013: Consequences of widespread tree mortality triggered by drought and temperature stress. *Nat. Climate Change*, **3**, 30–36, <https://doi.org/10.1038/nclimate1635>.
- Anderson, M. C., J. M. Norman, G. R. Diak, W. P. Kustas, and J. R. Mecikalski, 1997: A two-source time-integrated model for estimating surface fluxes using thermal infrared remote sensing. *Remote Sens. Environ.*, **60**, 195–216, [https://doi.org/10.1016/S0034-4257\(96\)00215-5](https://doi.org/10.1016/S0034-4257(96)00215-5).
- , —, J. R. Mecikalski, J. A. Otkin, and W. P. Kustas, 2007a: A climatological study of evapotranspiration and moisture stress across the continental United States based on thermal remote sensing: 1. Model formulation. *J. Geophys. Res.*, **112**, D10117, <https://doi.org/10.1029/2006JD007506>.
- , —, —, —, and —, 2007b: A climatological study of evapotranspiration and moisture stress across the continental United States based on thermal remote sensing: 2. Surface moisture climatology. *J. Geophys. Res.*, **112**, D11112, <https://doi.org/10.1029/2006JD007507>.
- , C. Hain, B. Wardlow, A. Pimstein, J. R. Mecikalski, and W. P. Kustas, 2011: Evaluation of drought indices based on thermal remote sensing of evapotranspiration over the continental United States. *J. Climate*, **24**, 2025–2044, <https://doi.org/10.1175/2010JCLI3812.1>.
- , and Coauthors, 2012: Mapping daily evapotranspiration at Landsat spatial scales during the BEAREX'08 field campaign. *Adv. Water Resour.*, **50**, 162–177, <https://doi.org/10.1016/j.advwatres.2012.06.005>.
- , C. Hain, J. Otkin, X. Zhan, K. Mo, M. Svoboda, B. Wardlow, and A. Pimstein, 2013: An intercomparison of drought indicators based on thermal remote sensing and NLDAS-2 simulations with U.S. Drought Monitor classifications. *J. Hydrometeorol.*, **14**, 1035–1056, <https://doi.org/10.1175/JHM-D-12-0140.1>.
- Baldocchi, D., and Coauthors, 2001: FLUXNET: A new tool to study the temporal and spatial variability of ecosystem-scale carbon dioxide, water vapor, and energy flux densities. *Bull. Amer. Meteor. Soc.*, **82**, 2415–2434, [https://doi.org/10.1175/1520-0477\(2001\)082<2415:FANTTS>2.3.CO;2](https://doi.org/10.1175/1520-0477(2001)082<2415:FANTTS>2.3.CO;2).
- Bell, J. E., and Coauthors, 2013: U.S. Climate Reference Network soil moisture and temperature observations. *J. Hydrometeorol.*, **14**, 977–988, <https://doi.org/10.1175/JHM-D-12-0146.1>.
- Bonan, G., 2002: *Ecological Climatology: Concepts and Applications*. Cambridge University Press, 678 pp.
- Budyko, M. I., 1974: *Climate and Life*. Academic Press, 508 pp.
- Campbell, G. S., and J. M. Norman, 1998: *An Introduction to Environmental Biophysics*. Springer Science & Business Media, 286 pp.
- Chen, F., and J. Dudhia, 2001: Coupling an advanced land surface–hydrology model with the Penn State–NCAR MM5 modeling system. Part I: Model implementation and sensitivity. *Mon. Wea. Rev.*, **129**, 569–585, [https://doi.org/10.1175/1520-0493\(2001\)129<0569:CAALSH>2.0.CO;2](https://doi.org/10.1175/1520-0493(2001)129<0569:CAALSH>2.0.CO;2).
- Crow, W. T., R. Dongryeol, and J. S. Famiglietti, 2005: Upscaling of field-scale soil moisture measurements using distributed land surface modeling. *Adv. Water Resour.*, **28**, 1–14, <https://doi.org/10.1016/j.advwatres.2004.10.004>.
- Czaja, A., and C. Frankignoul, 2002: Observed impact of Atlantic SST anomalies on the North Atlantic Oscillation. *J. Climate*, **15**, 606–623, [https://doi.org/10.1175/1520-0442\(2002\)015<0606:OIOASA>2.0.CO;2](https://doi.org/10.1175/1520-0442(2002)015<0606:OIOASA>2.0.CO;2).
- Dirmeyer, P. A., 2000: Using a global soil wetness dataset to improve seasonal climate simulation. *J. Climate*, **13**, 2900–2922, [https://doi.org/10.1175/1520-0442\(2000\)013<2900:UAGSWD>2.0.CO;2](https://doi.org/10.1175/1520-0442(2000)013<2900:UAGSWD>2.0.CO;2).
- , 2011: The terrestrial segment of soil moisture–climate coupling. *Geophys. Res. Lett.*, **38**, L16702, <https://doi.org/10.1029/2011GL048268>.
- , F. J. Zeng, A. Ducharne, J. C. Morrill, and R. D. Koster, 2000: The sensitivity of surface fluxes to soil water content in three land surface schemes. *J. Hydrometeorol.*, **1**, 121–134, [https://doi.org/10.1175/1525-7541\(2000\)001<0121:TSOSFT>2.0.CO;2](https://doi.org/10.1175/1525-7541(2000)001<0121:TSOSFT>2.0.CO;2).
- , X. Gao, M. Zhao, Z. Guo, T. Oki, and N. Hanasaki, 2006: GSWP-2: Multimodel analysis and implications for our perception of the land surface. *Bull. Amer. Meteor. Soc.*, **87**, 1381–1398, <https://doi.org/10.1175/BAMS-87-10-1381>.
- , C. A. Schlosser, and K. L. Brubaker, 2009: Precipitation, recycling, and land memory: An integrated analysis. *J. Hydrometeorol.*, **10**, 278–288, <https://doi.org/10.1175/2008JHM1016.1>.
- Ford, T. W., and S. M. Quiring, 2019: Comparison of contemporary in Situ, model, and satellite remote sensing soil moisture with a focus on drought monitoring. *Water Resour. Res.*, **55**, 1565–1582, <https://doi.org/10.1029/2018WR024039>.
- Frankignoul, C., and K. Hasselmann, 1977: Stochastic climate models, Part II Application to sea-surface temperature anomalies and thermocline variability. *Tellus*, **29**, 289–305, <https://doi.org/10.3402/Tellusa.V29I4.11362>.
- , A. Czaja, and B. L'Heveder, 1998: Air–sea feedback in the North Atlantic and surface boundary conditions for ocean models. *J. Climate*, **11**, 2310–2324, [https://doi.org/10.1175/1520-0442\(1998\)011<2310:ASFITN>2.0.CO;2](https://doi.org/10.1175/1520-0442(1998)011<2310:ASFITN>2.0.CO;2).
- Freund, R. J., W. J. Wilson, and D. L. Mohr, 2010: *Statistical Methods*. 3rd ed. Academic Press, 824 pp.
- Gevaert, A. I., D. G. Miralles, R. A. M. de Jeu, J. Schellekens, and A. J. Dolman, 2018: Soil moisture–temperature coupling in a set of land surface models. *J. Geophys. Res. Atmos.*, **123**, 1481–1498, <https://doi.org/10.1002/2017JD027346>.
- Grayson, R. B., and A. W. Western, 1998: Towards areal estimation of soil water content from point measurements: Time and space stability of mean response. *J. Hydrol.*, **207**, 68–82, [https://doi.org/10.1016/S0022-1694\(98\)00096-1](https://doi.org/10.1016/S0022-1694(98)00096-1).
- Hain, C. R., J. R. Mecikalski, and M. C. Anderson, 2009: Retrieval of an available water-based soil moisture proxy from thermal infrared remote sensing. Part I: Methodology and validation.

- J. Hydrometeorol.*, **10**, 665–683, <https://doi.org/10.1175/2008JHM1024.1>.
- Jacobs, J. M., B. P. Mohanty, E. Hsu, and D. Miller, 2004: SMEX02: Field scale variability, time stability and similarity of soil moisture. *Remote Sens. Environ.*, **92**, 436–446, <https://doi.org/10.1016/j.rse.2004.02.017>.
- Jarvis, P. G., 1976: The interpretation of the variations in leaf water potential and stomatal conductance found in canopies in the field. *Philos. Trans. Roy. Soc. London*, **B273**, 593–610, <https://doi.org/10.1098/rstb.1976.0035>.
- Karnieli, A., N. Agam, R. T. Pinker, M. Anderson, M. L. Imhoff, G. G. Gutman, N. Panov, and A. Goldberg, 2010: Use of NDVI and land surface temperature for drought assessment: Merits and limitations. *J. Climate*, **23**, 618–633, <https://doi.org/10.1175/2009JCLI2900.1>.
- Kaufmann, R., L. Zhou, R. B. Myneni, C. J. Tucker, D. Slayback, N. V. Shabanov, and J. Pinzon, 2003: The effect of vegetation on surface temperature: A statistical analysis of NDVI and climate data. *Geophys. Res. Lett.*, **30**, 2147, <https://doi.org/10.1029/2003GL018251>.
- Koster, R. D., and M. J. Suarez, 1999: A simple framework for examining the interannual variability of land surface moisture fluxes. *J. Climate*, **12**, 1911–1917, [https://doi.org/10.1175/1520-0442\(1999\)012<1911:ASFFET>2.0.CO;2](https://doi.org/10.1175/1520-0442(1999)012<1911:ASFFET>2.0.CO;2).
- , and —, 2001: Soil moisture memory in climate models. *J. Hydrometeorol.*, **2**, 558–570, [https://doi.org/10.1175/1525-7541\(2001\)002<0558:SMMICM>2.0.CO;2](https://doi.org/10.1175/1525-7541(2001)002<0558:SMMICM>2.0.CO;2).
- , and Coauthors, 2004: Regions of strong coupling between soil moisture and precipitation. *Science*, **305**, 1138–1140, <https://doi.org/10.1126/science.1100217>.
- , and Coauthors, 2006: GLACE: The Global Land–Atmosphere Coupling Experiment. Part I: Overview. *J. Hydrometeorol.*, **7**, 590–610, <https://doi.org/10.1175/JHMS10.1>.
- , S. D. Schubert, and M. J. Suarez, 2009: Analyzing the concurrence of meteorological droughts and warm periods, with implications for the determination of evaporative regime. *J. Climate*, **22**, 3331–3341, <https://doi.org/10.1175/2008JCLI2718.1>.
- , —, H. Wang, S. P. Mahanama, and A. M. DeAngelis, 2019: Flash drought as captured by reanalysis data: Disentangling the contributions of precipitation deficit and excess evapotranspiration. *J. Hydrometeorol.*, **20**, 1241–1258, <https://doi.org/10.1175/JHM-D-18-0242.1>.
- Lei, F., W. T. Crow, T. R. H. Holmes, C. Hain, and M. C. Anderson, 2018: Global investigation of soil moisture and latent heat flux coupling strength. *Water Resour. Res.*, **54**, 8196–8215, <https://doi.org/10.1029/2018WR023469>.
- Li, F., P. K. William, M. C. Anderson, J. H. Prueger, and R. L. Scott, 2008: Effect of remote sensing spatial resolution on interpreting tower-based flux observations. *Remote Sens. Environ.*, **112**, 337–349, <https://doi.org/10.1016/j.rse.2006.11.032>.
- Lian, T., Y. Tang, L. Zhou, S. U. Islam, C. Zhang, X. Li, and Z. Ling, 2018: Westerly wind bursts simulated in CAM4 and CCSM4. *Climate Dyn.*, **50**, 1353–1371, <https://doi.org/10.1007/s00382-017-3689-7>.
- Liu, Z., and N. Wen, 2008: On the assessment of nonlocal climate feedback. Part II: EFA-SVD and optimal feedback modes. *J. Climate*, **21**, 5402–5416, <https://doi.org/10.1175/2008JCLI2042.1>.
- , M. Notaro, J. Kutzbach, and N. Liu, 2006: Assessing global vegetation-climate feedbacks from observations. *J. Climate*, **19**, 787–814, <https://doi.org/10.1175/JCLI3658.1>.
- , N. Wen, and Y. Liu, 2008: On the assessment of nonlocal climate feedback. Part I: The generalized equilibrium feedback assessment. *J. Climate*, **21**, 134–148, <https://doi.org/10.1175/2007JCLI1826.1>.
- Lozano-Parra, J., M. Pulido, C. Lozano-Fondón, and S. Schnabel, 2018: How do soil moisture and vegetation covers influence soil temperature in drylands of Mediterranean regions? *Water*, **10**, 1747, <https://doi.org/10.3390/w10121747>.
- McKee, T. B., N. J. Doesken, and J. Kleist, 1993: The relationship of drought frequency and duration to time scales. *Proc. Eighth Conf. on Applied Climatology*, Anaheim, CA, Amer. Meteor. Soc., 179–184.
- McNaughton, K. G., and T. W. Spriggs, 1986: A mixed-layer model for regional evaporation. *Bound.-Layer Meteorol.*, **34**, 243–262, <https://doi.org/10.1007/BF00122381>.
- Mecikalski, J. R., W. B. Shoemaker, Q. Wu, and M. A. Holmes, 2018: High-resolution GOES insolation-evapotranspiration data set for water resource management in Florida: 1995–2015. *J. Irrig. Drain. Eng.*, **144**, 04018025, [https://doi.org/10.1061/\(ASCE\)IR.1943-4774.0001312](https://doi.org/10.1061/(ASCE)IR.1943-4774.0001312).
- Miralles, D. G., M. J. van den Berg, A. J. Teuling, and R. A. M. de Jeu, 2012: Soil moisture-temperature coupling: A multiscale observational analysis. *Geophys. Res. Lett.*, **39**, L21707, <https://doi.org/10.1029/2012GL053703>.
- Mohanty, B. P., and T. H. Skaggs, 2001: Spatio-temporal evolution and time-stable characteristics of soil moisture within remote sensing footprints with varying soil, slope, and vegetation. *Adv. Water Resour.*, **24**, 1051–1067, [https://doi.org/10.1016/S0309-1708\(01\)00034-3](https://doi.org/10.1016/S0309-1708(01)00034-3).
- Mueller, B., and S. I. Seneviratne, 2012: Hot days induced by precipitation deficits at the global scale. *Proc. Natl. Acad. Sci. USA*, **109**, 12 398–12 403, <https://doi.org/10.1073/pnas.1204330109>.
- Myneni, R. B., C. J. Tucker, G. Asrar, and C. D. Keeling, 1998: Interannual variations in satellite-sensed vegetation index data from 1981 to 1991. *J. Geophys. Res.*, **103**, 6145–6160, <https://doi.org/10.1029/97JD03603>.
- , and Coauthors, 2002: Global products of vegetation leaf area and fraction absorbed PAR from year one of MODIS data. *Remote Sens. Environ.*, **83**, 214–231, [https://doi.org/10.1016/S0034-4257\(02\)00074-3](https://doi.org/10.1016/S0034-4257(02)00074-3).
- Nadelhoffer, K. J., A. E. Giblin, G. R. Shaver, and J. L. Laundre, 1991: Effects of temperature and substrate quality on element mineralization in six arctic soils. *Ecology*, **72**, 242–253, <https://doi.org/10.2307/1938918>.
- Nievola, C. C., C. P. Carvalho, V. Carvalho, and E. Rodrigues, 2017: Rapid responses of plants to temperature changes. *Temperature*, **4**, 371–405, <https://doi.org/10.1080/2328940.2017.1377812>.
- Norman, J. M., W. P. Kustas, and K. S. Humes, 1995: Source approach for estimating soil and vegetation energy fluxes in observations of directional radiometric surface temperature. *Agric. For. Meteorol.*, **77**, 263–293, [https://doi.org/10.1016/0168-1923\(95\)02265-Y](https://doi.org/10.1016/0168-1923(95)02265-Y).
- Notaro, M., Z. Liu, and J. W. Williams, 2006: Observed vegetation-climate feedbacks in the United States. *J. Climate*, **19**, 763–786, <https://doi.org/10.1175/JCLI3657.1>.
- Otkin, J. A., M. C. Anderson, C. Hain, and M. Svoboda, 2014: Examining the relationship between drought development and rapid changes in the evaporative stress index. *J. Hydrometeorol.*, **15**, 938–956, <https://doi.org/10.1175/JHM-D-13-0110.1>.
- , —, —, and —, 2015a: Using temporal changes in drought indices to generate probabilistic drought intensification forecasts. *J. Hydrometeorol.*, **16**, 88–105, <https://doi.org/10.1175/JHM-D-14-0064.1>.
- , M. Shafer, M. Svoboda, B. Wardlow, M. C. Anderson, C. Hain, and J. Basara, 2015b: Facilitating the use of drought early warning information through interactions with agricultural

- stakeholders. *Bull. Amer. Meteor. Soc.*, **96**, 1073–1078, <https://doi.org/10.1175/BAMS-D-14-00219.1>.
- , Y. Zhong, D. Lorenz, M. C. Anderson, and C. Hain, 2018: Exploring seasonal and regional relationships between the Evaporative Stress Index and surface weather and soil moisture anomalies across the United States. *Hydrol. Earth Syst. Sci.*, **22**, 5373–5386, <https://doi.org/10.5194/hess-22-5373-2018>.
- Palmer, W. C., 1965: Meteorological drought. U.S. Weather Bureau Research Paper 45, 58 pp., <http://www.ncdc.noaa.gov/temp-and-precip/drought/docs/palmer.pdf>.
- Saha, S., and Coauthors, 2010: The NCEP Climate Forecast System Reanalysis. *Bull. Amer. Meteor. Soc.*, **91**, 1015–1057, <https://doi.org/10.1175/2010BAMS3001.1>.
- Salvucci, G. D., J. A. Saleem, and R. Kaufmann, 2002: Investigating soil moisture feedbacks on precipitation with tests of Granger causality. *Adv. Water Resour.*, **25**, 1305–1312, [https://doi.org/10.1016/S0309-1708\(02\)00057-X](https://doi.org/10.1016/S0309-1708(02)00057-X).
- Seneviratne, S. I., D. Luthi, M. Litschi, and C. Schar, 2006a: Land-atmosphere coupling and climate change in Europe. *Nature*, **443**, 205–209, <https://doi.org/10.1038/nature05095>.
- , and Coauthors, 2006b: Soil moisture memory in AGCM simulations: Analysis of Global Land-Atmosphere Coupling Experiment (GLACE) data. *J. Hydrometeorol.*, **7**, 1090–1112, <https://doi.org/10.1175/JHM533.1>.
- , T. Corti, E. L. Davin, M. Hirschi, E. B. Jaeger, I. Lehner, B. Orlowsky, and A. J. Teuling, 2010: Investigating soil moisture–climate interactions in a changing climate: A review. *Earth-Sci. Rev.*, **99**, 125–161, <https://doi.org/10.1016/j.earscirev.2010.02.004>.
- Short Gianotti, D. J., G. D. Salvucci, R. Akbar, K. A. McColl, R. Cuenca, and D. Entekhabi, 2019: Landscape water storage and subsurface correlation from satellite surface soil moisture and precipitation observations. *Water Resour. Res.*, **55**, 9111–9132, <https://doi.org/10.1029/2019WR025332>.
- Sugihara, G., R. May, H. Ye, C. Hsieh, E. Deyle, M. Fogarty, and S. Munch, 2012: Detecting causality in complex ecosystems. *Science*, **338**, 496–500, <https://doi.org/10.1126/science.1227079>.
- Teuling, A. J., and S. I. Seneviratne, 2008: Contrasting spectral changes limit albedo impact on land-atmosphere coupling during the 2003 European heat wave. *Geophys. Res. Lett.*, **35**, L03401, <https://doi.org/10.1029/2007GL032778>.
- , and Coauthors, 2009: A regional perspective on trends in continental evaporation. *Geophys. Res. Lett.*, **36**, L02404, <https://doi.org/10.1029/2008GL036584>.
- Tuttle, S. E., and G. D. Salvucci, 2017: Confounding factors in determining causal soil moisture–precipitation feedback. *Water Resour. Res.*, **53**, 5531–5544, <https://doi.org/10.1002/2016WR019869>.
- Vicente-Serrano, S. M., S. Begueria, and J. I. Lopez-Moreno, 2010: A multiscale drought index sensitive to global warming: The standardized precipitation evapotranspiration index. *J. Climate*, **23**, 1696–1718, <https://doi.org/10.1175/2009JCLI2909.1>.
- von Storch, H., and F. W. Zwiers, 1999: *Statistical Analysis in Climate Research*. Cambridge University Press, 499 pp.
- Wilson, T. B., C. B. Baker, T. P. Meyers, J. Kochendorfer, M. Hall, J. E. Bell, H. J. Diamond, and M. A. Palecki, 2016: Site-specific soil properties of the US climate reference network soil moisture. *Vadose Zone J.*, **15** (11), 1–14, <https://doi.org/10.2136/VZJ2016.05.0047>.
- Xia, Y., M. Ek, H. Wei, and J. Meng, 2012a: Comparative analysis of relationships between NLDAS-2 forcings and model outputs. *Hydrol. Processes*, **26**, 467–474, <https://doi.org/10.1002/hyp.8240>.
- , and Coauthors, 2012b: Continental-scale water and energy flux analysis and validation for the North American Land Data Assimilation System project phase 2 (NLDAS-2): 1. Intercomparison and application of model products. *J. Geophys. Res.*, **117**, D03109, <https://doi.org/10.1029/2011JD016048>.
- Zhong, Y., and Z. Liu, 2009: On the mechanism of Pacific multi-decadal climate variability in CCSM3: The role of the subpolar North Pacific Ocean. *J. Phys. Oceanogr.*, **39**, 2052–2076, <https://doi.org/10.1175/2009JPO4097.1>.
- , —, and M. Notaro, 2011: A GEFA assessment of observed global ocean influence on U.S. Precipitation variability: Attribution to regional SST variability modes. *J. Climate*, **24**, 693–707, <https://doi.org/10.1175/2010JCLI3663.1>.